Analyst

PAPER

View Article Online
View Journal

Cite this: DOI: 10.1039/d0an01054e

An off/on thrombin activated energy driven molecular machine for sensitive detection of human thrombin *via* non-enzymatic catalyst recycling amplification†

Zhang Zhang, [a] Min Mei,[a] Juan Yao, [b] Ting Ye,[a] Jing Quan[a] and Jinbo Liu *[a]

Received 26th May 2020,
Accepted 10th June 2020

DOI: 10.1039/d0an01054e

rsc.li/analyst

In this article, we report a novel dual on/off thrombin fluorescence aptasensor by combining the energy driven target induced strand displacement reaction and a non-enzyme catalyst recycling DNA machine. Firstly, the specific binding of an aptamer strand and thrombin induce the release of a catalyst which was used as a DNA machine trigger. Subsequently, the catalyst as the trigger initiated the DNA machine through nucleic acid hybridization and branch migration of the DNA machine, resulting in the DNA substrate melting and re-hybridization. In such a working model, the DNA machine achieved cooperative control of the circular strand displacement reaction, realizing catalyst recycling and dual-amplification. The fluorescence signal change of FAM and ROX accumulation had a good linear relationship with the thrombin concentration in the range of 1 fM to 1 nM. On account of catalyst recycling and dual recognition, the detection limit for thrombin was determined to be as low as 0.45 fM (S/N = 3).This biosensor also showed good selectivity for thrombin without being affected by some other proteins, such as PSA, lysozyme *etc.* Moreover, this assay can be applied to the detection of thrombin in diluted human serum.

Introduction

The detection of proteins plays an essential role in fundamental research and in the diagnosis of diseases. Thrombin is a specific serine endoprotease that plays an essential role in many life processes such as blood coagulation, angiogenesis and wound healing processes.[1–3] Due to protein low abundance, developing sensitive protein detection techniques and methods has been a bottleneck of proteomics development.[4,5] Therefore, many researchers converted the detection of proteins into the detection of nucleic acids for dramatically improving the sensitivity of protein detection. The developed protein detection methods include immuno-PCR,[6] affinity aptamer PCR,[7] immuno-T7 RNA polymerase amplification techniques,[8] catalytic hairpin self-assembly,[9] rolling circle amplification,[10] hybridization chain reaction[11] and proximity-dependent amplification.[12]

To date antibody bio-recognition element based assays including standard enzyme immunoassay,[13] immuno-electrochemiluminescence[14] and immuno-luminescence[15] are the most commonly used diagnostic methods. Recently, a new class of receptors called aptamers has emerged and they show excellent potential for application in protein analysis. Aptamers are single-stranded DNA or RNA oligonucleotides generated by systematic evolution of ligands by the exponential enrichment (SELEX) process. The variable sequence confers each aptamer with a unique dimensional structure and potential ligand binding capability, and it can specifically recognize and bind to a variety of diagnostically relevant marker molecules including proteins, small molecules and even cells.[16–18] The different nature of these nucleic-acid recognition elements and their protein targets, and the unique properties of aptamers show great promise for designing innovative sensing protocols. In comparison with antibodies, aptamers show such advantages as high affinity, temperature insensitivity, and stability when exposed to a wide range of chemicals, long shelf lives, simple chemical synthesis and low cost. These characteristics make aptamers a useful tool in diagnostics, analytical and therapeutic fields. Conventional immunoassays for thrombin have several disadvantages, including lengthy assay time, labor-intensive protocol, and high sample/reagent consumption. Recently, an aptamer-based protein assay has shown great promise for designing innovative sensing protocols including optical and electrochemical sensing in thrombin assays.[19]

Sensitivity and dynamic range are the main factors used for evaluating a method. The limit of detection need to be low

[a]Department of Laboratory Medicine, The Affiliated Hospital of Southwest Medical University, Luzhou, China. E-mail: liulab2019@163.com
[b]Department of Laboratory Medicine, The Affiliated Traditional Chinese Medicine Hospital of Southwest Medical University, Luzhou, China

†Electronic supplementary information (ESI) available: Fig. S1–S6 and Tables S1–S5. See DOI: 10.1039/d0an01054e

enough to ensure sensitivity, and the dynamic range covering the entire useful concentrations may be more important for some specific applications such as routine monitoring of diseases. In order to improve the sensitivity, various methods mainly including target or signal amplification were used, for instance, nanomaterials,[20,21] nucleic acid isothermal amplification technologies[22,23] and enzyme based methods.[24,25] Among them, a toehold-mediated strand displacement reaction (SDR) based target recycling molecular machine attracts great interest because it is extremely simple, enzyme-free, and reacts in homogeneous solution without any immobilization, separation and washing steps.[26–29] The SDR which was pioneered by Yurke *et al.*[30] for its application in DNA nanotechnology with the demonstration of dynamic DNA tweezers involves the displacement of a DNA strand from a dsDNA duplex with a single-stranded overhang called toehold by an oligonucleotide that is fully complementary to the longer strand of the duplex starting from the toehold region. An SDR based molecular machine was originally developed by Pierce, Yin, and co-workers in their seminal work[31] and has been adaptable to multiple detection methods for analyzing nucleic acids and small molecules. The SDR (contains three steps: toehold domains initiate binding, branch migration and strand displacement is completed; see Fig. S1†) utilizes double-strand DNA with thermodynamic properties to enable near-optimal single nucleotide discrimination and perform robustly under diverse temperature, salt and concentration conditions. SDR based target recycling is a spontaneous phenomenon driven forward by entropy without any enzymes. So far, it had been applied in nucleic acid detection, DNA digital circuit computation, DNA-based molecular circuits and DNA nanoswitches. Unlike previously reported hybridization-based catalyst systems such as catalytic hairpin assembly,[32,33] this reaction design does not require unusual secondary structures such as pseudoknots and kissing loops. This merit has made the design and realization of this molecular machine easy.

Aiming to develop a versatile fluorescence thrombin biosensor with acceptable sensitivity and dynamic range, target protein-induced strand displacement and SDR based target recycling were used for target and signal amplification. An SDR based target recycling molecular machine coupled with cascade signal amplification endues high sensitivity of the developed fluorescence biosensor. The enzyme-free amplification strategy eliminates the requirement for any protein enzymes, making the system suitable for one step homogeneous analysis in a tube without open. This developed biosensing strategy presented a simple and stable platform toward sensitive and convenient thrombin detection, and had great potential in assays of many other biological analytes for biomedical research and early clinical diagnosis.

Experimental section

Materials and apparatus

DNA oligonucleotides and thrombin aptamers were synthesized and HPLC purified by Sangon Inc. (Shanghai, China) and their sequences are listed in Table S1† and domains are shown in Table S2.† All oligonucleotides were dissolved in Tris-EDTA (TE) buffer (pH 8.0, 10 mM Tris–HCl, 1 mM EDTA) and stored at −20 °C before use. Tris-HCl (pH 7.0, containing 200 mM NaCl) was used as hybridization buffer throughout all experiments. Thrombin was purchased from Sigma-Aldrich (St Louis, USA), and prostate specific antigen (PSA), carcinoembryonic antigen (CEA) alpha-fetoprotein (AFP), procalcitonin (PCT), HBsAg, and lysozyme were purchased from Biocell Biotech. Co., Ltd (Zhengzhou, China). A thrombin ELISA kit was obtained from BioVision Incorporated (San Francisco, USA). All other reagents were of analytical grade and were used without further purification. Ultrapure water (Milli-Q 18.2 MΩ cm^2, Millipore System Inc.) was used for all the experiments. All spectrofluorometric measurements were performed with an Enspire multimode microplate reader (PerkinElmer, USA). The excitation/emission for FAM and ROX were recorded at 480/518 and 570/607 nm and kinetics was measured every 30 seconds using an 8-well polystyrene strip plate (Corning Incorporated, USA). An electrophoresis apparatus (LIUYI Corporation, China) was used in the PAGE gel electrophoresis experiment. Gel image was recorded by using an imaging system (Bio-Rad Laboratories, USA).

DNA sequences and design

For thrombin target protein-induced strand displacement, the secondary structure and standard Gibbs energy change (ΔG°) of the aptamer was analyzed using UNAfold software online.[34] The catalyst strand as a protector was chosen rationally to ensure target protein-induced strand displacement, thus ensuring acceptable selectivity and sensitivity. For catalyst strand initiated non-enzymatic target recycling amplification, DNA sequences and modifications are based on a DNA strand displacement reported by Zhang *et al.*[35] and modified by hand to generate allosteric toehold sequences (sequences and domains are shown in Tables S1 and S2, and energy change is shown in Table S3†). All DNA sequences were then analyzed using UNAfold to ensure minimal crosstalk between unrelated domains. All DNA oligonucleotides were denatured at 95 °C for 5 min and cooled down at 5 °C per minute to room temperature.

Fabrication and characterization of the fluorescence biosensor

For the characterization and optimization of the thrombin mediated strand displacement reaction, 50 μL of 1 μM aptamer/catalyst duplex was first injected into a plate, followed by the injection of different concentrations of thrombin. Fluorescence emission spectra were recorded at the optimal time. For the characterization of catalyst initiated DNA recycling, 25 μL of 800 nM three-strand DNA complex substrate and an equal volume of 25 μL of 800 nM fuel strand were mixed, followed by the injection of 50 μL of 1 nM catalyst to confirm the signal amplification effect.

For the preparation of the reaction mixture, 30 μL of 600 nM three-strand DNA complex substrate, and 30 μL of fuel and 30 nM aptamer/catalyst strand were first injected into an 8-well

polystyrene strip plate, followed by the injection of 10 μL of paraffins (to prevent the reaction between thrombin target and the reaction mixture before monitoring in real-time fluorescence records). The reaction mixture was then stored at −20 °C before use. Different concentrations of thrombin target were added to the reaction tube and an Enspire multimode microplate reader was used to monitor the real-time fluorescence change immediately.

Results and discussion

The working principle of the proposed biosensor

The principle of our thrombin-activated DNA machine for nonenzymatic and amplified fluorescence detection of thrombin is illustrated in Scheme 1. As shown in Scheme 1A, in the absence of thrombin, the aptamer and catalyst strands were firmly tethered to form a duplex, whereas in the presence of thrombin target, the aptamer mediated strand displacement reaction occurred and resulted in the release of the catalyst strand as the circuit amplification input and then a catalyst strand triggered molecular machine for non-enzymatic target recycling amplification. To further illustrate this thrombin mediated strand displacement reaction, mole fractions of the aptamer and catalyst were computed as a function of temperature (Fig. S2†) and their secondary structures were predicted using UNAfold and are shown in Fig. S3†. Specifically, and as shown in Scheme 1B, the sensing system is composed of a three-strand DNA complex substrate (S) and a fuel strand (F). The three-strand DNA complex substrate is composed of a linker strand (L) coupled assistant probe (AP) and a signal probe (SP). Strands are conceptually subdivided into functional domains (domains are shown in different colors and sequences are given in Table S2†), whose sequences determine the pattern of interactions between the circuit components. As shown in Scheme 1C, in the presence of the catalyst strand as the trigger, the catalyst first binds to the single-stranded toehold domain d on the substrate to form a four-stranded intermediate (I1), which is inherently unstable and then rearranges *via* branch migration to form I2. The binding between toehold domains b and b* is too weak to keep the SP connected to I2, spontaneously dissociating into AP and I3. Newly exposed b* then facilitates the binding of the fuel strand, resulting in I4, which then quickly rearranges to release the signal probe and I5. Finally, I5 rearranges so that the catalyst is attached only by the binding of d and d*, which spontaneously dissociates to leave waste and regenerate the catalyst. This procedure separates the SP from the linker, and makes the fluorophore (ROX) become fluorescent, whereas the fuel strand close to the linker makes the fluorophore (FAM) quenched. The above changes lead to the increase of the ROX fluorescence signal and decrease of the FAM fluorescence signal thus contributing to this "signal-on/off" sensing system. The catalyst is thus recycled and it initiates the DNA machine fueled by the fuel strand, causing the release of a large number of SPs from the substrate and significantly amplified fluorescent signals for achieving highly sensitive detection of thrombin.

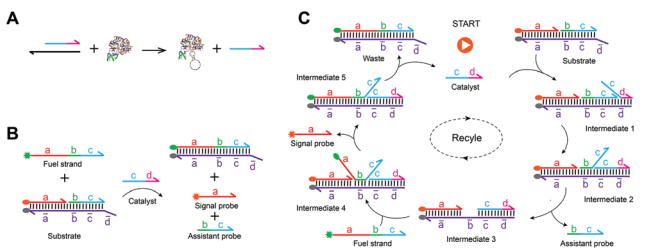

Scheme 1 (A) Illustration of thrombin activated strand displacement reaction to generate the catalyst. (B) Illustration of the dual-signal fluorescence detection of thrombin using cascade toehold-mediated strand displacement along with non-enzymatic catalyst recycling amplification. (C) Detailed branch migration procedure of (B).

Characterization and feasibility of the biosensor

The feasibility of thrombin target mediated strand displacement was confirmed and is shown in Fig. 1. As shown in Fig. 1A and B, catalyst labels FAM shows high fluorescence signal (curve a). When aptamer strand hybridized with catalyst and formed duplex, non fluorescence was observed due to fluorescence resonance energy transfer (FRET, curve b). As shown in curve c, a high fluorescence signal was obtained in the presence of thrombin, because the affinity between thrombin/aptamer is stronger than the aptamer/catalyst complexes, thus separating the quencher and fluorophore. In contrast,

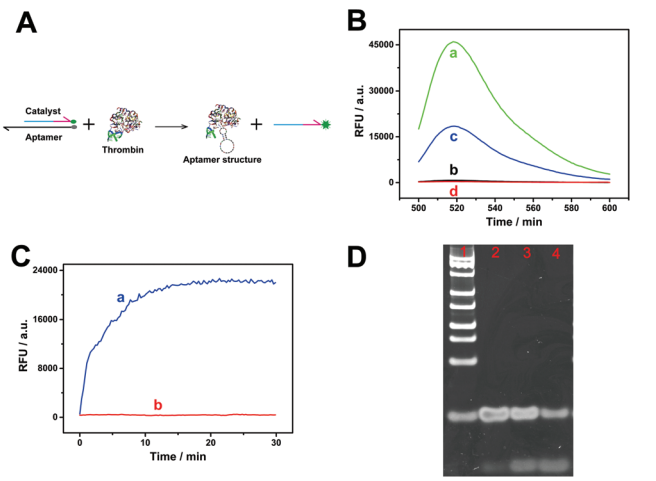

Fig. 1 (A) Scheme of thrombin activated strand displacement reaction to generate the catalyst and (B) characterization of thrombin mediated strand displacement reaction. Curve a: 1 μM catalyst strand; curve b: 500 nM catalyst/aptamer duplex; curve c: 500 nM aptamer/catalyst added 500 nM thrombin; and curve d: 500 nM aptamer/catalyst added hybridization buffer. (C) Kinetics response of 500 nM aptamer/catalyst added 500 nM thrombin (curve a) and the negative control (curve b). (D) Native PAGE electrophoresis image of the performance of aptamer-affinity process, from left to right: 25 bp marker (lane 1); 500 nM aptamer/catalyst (lane 2); 500 nM aptamer/catalyst + 200 nM thrombin (lane 3); 500 nM aptamer/catalyst + 500 nM thrombin (lane 4).

when hybridization buffer was injected as the negative control, no obvious signal change was observed compared with the curve c. The standard Gibbs energy change for the thrombin activated strand displacement reaction was calculated by using the following steps: the equation of aptamer mediated strand displacement reaction can be expressed as A + B = C + D (where A represents the aptamer/catalyst complex, B represents thrombin, C represents the catalyst and D represents the aptamer/thrombin complex; K_{on} and K_{off} represent the rate constants of the forward and reverse reaction, respectively). The reaction is in equilibrium when the concentrations do not change:

$$[A] \cdot [B] \cdot K_{on} - [C] \cdot [D] \cdot K_{off} = 0 \quad \text{(mass action law)},$$

then transformed as:

$$[A] \cdot [B] \cdot K_{on} = [C] \cdot [D] \cdot K_{off} \quad \text{(equilibrium is reached and still dynamic)}$$

Rearrange the equation to define the equilibrium dissociation constant K_d:

$$K_d = \frac{K_{off}}{K_{on}} = \frac{[A] \cdot [B]}{[C] \cdot [D]} = \exp\left(\frac{\Delta G^\circ}{RT}\right)$$

Thus K_d was calculated to be 0.041 and ΔG° was calculated to be −1.89 kcal mol^{-1} (It should be noted that K_d here is calculated in the aptamer mediated strand displacement reaction. Note that for a reaction with different numbers of reactants and products, K_d is not unitless, and its value will depend on its unit). Thus, ΔG of a reaction may depend on the units used for expressing K_d. The above results indicated the feasibility of the thrombin target mediated strand displacement reaction and the high affinity of thrombin/aptamer conjugates. Fig. 1C shows the kinetics of the thrombin mediated strand displacement reaction to further illuminate this reaction. The thrombin mediated strand displacement reaction seems to reach equilibrium (curve a) after 10 min, whereas no obvious signal was observed when hybridization buffer was added as the negative control (curve b). Native PAGE electrophoresis was further used to confirm the aptamer detection strategy. As shown in Fig. 1D, the aptamer/catalyst duplex showed distinct bands (lane 2); when a bit amount of thrombin was added, the catalyst strand was released and a relatively dull band was observed (lane 3); by increasing the concentration of thrombin, a relatively bright band was observed (lane 4). The above results indicate the feasibility of the thrombin mediated strand displacement reaction.

SDR based catalyst recycling was then confirmed. As shown in Fig. 2A, for the signal-on model, the substrate shows no obvious signal due to the close distance between Dabcyl and ROX (curve c), the reason for which may be that the SP and AP sealed the active domain so the fuel cannot replace them. After adding the catalyst strand, the non-enzymatic molecular machine was triggered and a significant increase in the fluorescence intensity was observed (curve c *vs.* curve d). Such an increase is basically due to the target recycling signal amplification as discussed previously. Similar results were observed in the signal-off model and the changes were in good agreement with those in the signal-on model (curve a *vs.* curve b), which further demonstrated that the ROX labeled signal probe acted as a "signal-on" probe in this sensing system, whereas the FAM labeled fuel strand acted as a "signal-off" probe. A similar result of kinetics was observed further illustrating this signal on/off strategy (see in Fig. 2B). Native PAGE electrophoresis was also used to characterize the process of isothermal amplification reaction (see in Fig. 2C). The substrate and fuel strand showed two individual bands because when the catalyst was added to the reaction mixture, the strand displacement based target reaction occurred and the new broad AP and SP strands were released. The above electrophoresis results suggested that a right catalyst strand input could trigger strand displacement reaction based target recycling. The secondary structures of the substrate, intermediate 3 and waste were predicted by NUPACK (http://www.nupack.org/) and are shown in Fig. 2D–F. In conclusion, this developed DNA machine produced a readily measured fluorescence signal variation that could be related to the presence and concentration of the catalyst and thus can be used for the detection of thrombin.

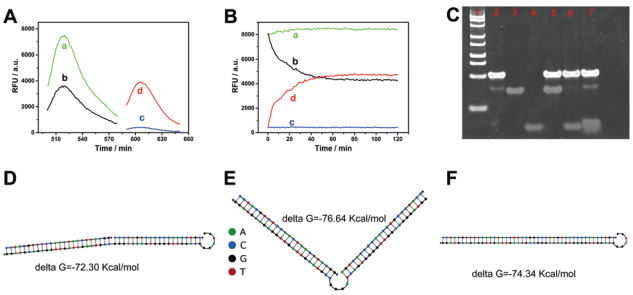

Fig. 2 Characterization of SDR based target recycling molecular machine. Fluorescence emission spectrum (A) and kinetics response (B) of SDR based molecular machine: FAM signal of 200 nM substrate and fuel (curve a); added 1 nM catalyst (curve b); ROX signal of 200 nM substrate and fuel (curve c); added 1 nM catalyst (curve d); (C) native-PAGE electrophoresis analysis of the feasibility of SDR based molecular machine: lane 1: 25 bp marker; lane 2: 500 nM substrate; lane 3: 500 nM fuel; lane 4: 500 nM catalyst; lane 5: 500 nM substrate and 500 nM fuel; lane 6: 500 nM substrate and 500 nM catalyst; and lane 7: 500 nM substrate, 500 nM fuel and 500 nM catalyst; and the predicted secondary structures of substrate (D), intermediate 3 (E) and waste (F).

Optimization of the reaction conditions

To achieve the perfect sensing performance of thrombin analysis, the cyclic cascade amplification reaction conditions were systematically investigated including the incubation time, incubation temperature, concentration of fuel strand, concentration of SP/AP/L substrate, aptamer/catalyst duplex concentration and pH. When a reaction condition was optimized, the other conditions were maintained at optimized conditions or

the longest reaction times and the highest concentrations were used. As shown in Fig. 3A, the fluorescence signal increased with the augment of the reaction duration because the massive substrate probe were separated. The maximum signal was observed when the reaction was carried out for about 120 min. Temperature is another factor that influences the results of this strategy. For nucleic acid hybridization, relatively high temperature may accelerate the toehold-mediated SDR and much more high temperature may denature double-stranded DNA thus leading to deteriorate results. For the combination of the aptamer and target, temperature may influence the secondary structures of the aptamer and even the denaturalized protein target. Fig. 3B shows the enrichment performance of the system across reaction temperatures ranging between 15 and 35 °C, where below 25 °C, the DNA hybridization activity decreases, resulting in poor amplification; above 25 °C, the hybridization between DNA becomes unstable, also resulting in deteriorate amplification. The relative broad temperature robustness of this proposed DNA machine manifests as a strong advantage in the design and operation for easily replacing other targets. Considering that a relatively high temperature may lead to a deteriorative background signal, we chose 25 °C as the optimal condition. As shown in Fig. 3C and D, the concentration of the fuel strand and concentration of the SP/AP/L substrate were also confirmed. The results indicated that the optimal concentration of the fuel strand was 200 nM and that of the SP/AP/L substrate was 200 nM. As illustrated in Fig. S4A,† the no color filling pillar represented the fluorescence variation obtained in the presence of thrombin. The color filling pillar represented the background signal. The results indicated that the optimal concentration of the aptamer/catalyst duplex was 10 nM. As observed in Fig. S4B,† the fluorescence signal reached a maximum when the pH was 7.0. Besides, the pH of healthy human blood is neutral. Therefore, the Tris–HCl buffer solution with pH 7.0 was chosen for the experiments.

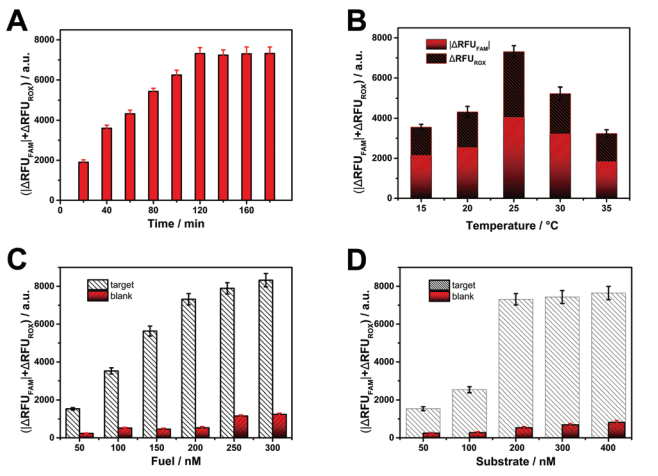

Fig. 3 Optimization of the experimental conditions. Effects of (A) reaction duration time; (B) temperature; (C) concentration of fuel strand and (D) concentration of SP/AP/L substrate. Error bars represented standard deviations of the measurements (n = 3).

The dynamic range, sensitivity and selectivity of the proposed nanomachine

To investigate the sensitivity and dynamic range of the proposed non-enzyme DNA thrombin aptamer biosensor, various concentrations of thrombin were incubated and the corresponding fluorescence signals were recorded under optimal conditions. As depicted in Fig. 4A, it could be observed that the peak of FAM intensity decreased and the ROX signal intensity increased with a gradual increase in the concentration of thrombin from 1 fM to 1 nM. As shown in Fig. 4B, both of the resulting calibration curves exhibited a linear relationship in the range of 0 to 6, and the detection limits were 0.60 and 0.75 fM (S/N = 3), corresponding to the FAM and ROX signals respectively. To amplify the fluorescence response, ΔF_{ROX} + $|\Delta F_{FAM}|$ was used as the response signal to determine quantitatively the concentration of thrombin (Fig. 4C). The value of ΔF_{ROX} + $|\Delta F_{FAM}|$ was linear with the logarithm of thrombin concentration (Fig. 4D). The regression equation was expressed as ΔF_{ROX} + $|\Delta F_{FAM}|$ = 1723.7 × log C (fM) + 1836.3 with a coefficient of determination (R^2) of 0.997, where C is the concentration of thrombin (n = 3). The detection limit was estimated to be 0.45 fM (S/N = 3). That means 1.4 × 10^2 to 2.9 × 10^7 amplification ratio for different concentrations of thrombin (see Fig. S5†). Obviously, the proposed method in this study

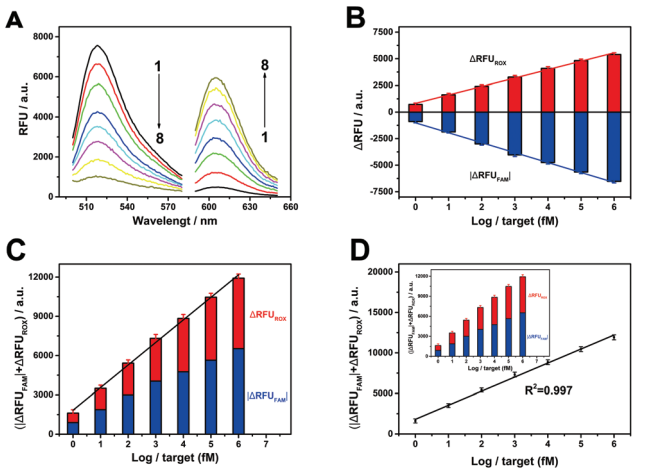

Fig. 4 Analytical performance of the aptamer biosensor. (A) RFU of the "signal-on/off" system with the increasing concentrations of thrombin (from 1 to 8: 0, 1 fM, 10 fM, 100 fM, 1 pM, 10 pM, 100 pM and 1 nM, respectively). (B) $|\Delta RFU_{FAM}|$ and ΔRFU_{ROX}, (C) $|\Delta RFU_{FAM}|$ + ΔRFU_{ROX} on the logarithm of thrombin concentration. The regression equation was expressed as $|\Delta RFU_{FAM}|$ = 935.7 × log C (fM) + 1010.7 with a coefficient of determination (R^2) of 0.996 and ΔRFU_{ROX} = 788.1 × log C (fM) + 826.5, with a coefficient of determination (R^2) of 0.996, where C is the concentration of thrombin. (D) Calibration curve of ΔF_{ROX} + $|\Delta F_{FAM}|$ *versus* the logarithm of thrombin concentrations. Inset: the relationship between the ΔF_{ROX} + $|\Delta F_{FAM}|$ and the concentrations of thrombin. Error bars represented standard deviations of the measurements (n = 3).

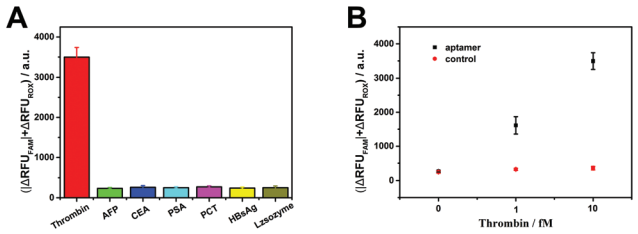

Fig. 5 (A) Selectivity evaluation for the detection of thrombin (10 fM) against10-fold 100 fM concentrations of AFP, CEA, PSA, PCT, HBsAg and lysozyme at the same concentration. (B) Sequence specificity test by using the aptamer control. The error bars were standard deviations of three independent measurements.

showed good performance in terms of analytical range and detection limit. In comparison with the commercial ELISA (see Fig. S6†) and some recently published works (see Table S4†), this aptasensor exhibited a comparable dynamic range and lower detection limit.

Besides sensitivity, the selectivity of this method for thrombin detection was also investigated. Glucose in addition to other proteins including AFP, CEA, PSA, PCT, HBsAg and lysozyme with the same concentrations as 10-fold 100 fM and 10 fM thrombin were employed to investigate the selectivity of the aptasensor. The results obtained are displayed and compared in Fig. 5A. Significant changes were observed only in the presence of 10 fM thrombin. However, there was almost no signal change of fluorescence when 10-fold 100 fM concentration of these control proteins were added. It is clearly demonstrated that in the presence of other proteins including AFP, CEA, PSA, PCT, HBsAg and lysozyme, no obvious change was observed. The sequence specificity of the thrombin aptamer was also tested by assessing thrombin with the aptamer control. In the control experiment, we did not observe significant signal increase in the presence of thrombin (Fig. 5B). The above results indicated that the proposed aptasensor displayed good specificity for the detection of thrombin.

Thrombin detection in human blood samples

To further demonstrate whether the method was applicable in real bio-environments, we mixed three concentrations of thrombin (10 fM, 100 fM and 1000 fM) with diluted healthy human serum obtained from affiliated hospital of Southwest Medical University. All experiments were performed in accordance with the guidelines and approved by the ethics committee at affiliated hospital of Southwest Medical University. Informed consents were obtained from human participants of this study. The assay results were compared with that of buffer solution (see Table S5†). It was suggested that this target protein-induced strand displacement and SDR based target recycling method has the ability to detect thrombin in a complex matrix, and it might become a promising candidate tool for clinical diagnosis.

Conclusions

In conclusion, we have demonstrated a versatile fluorescence aptamer biosensor with high sensitivity and relatively wide dynamic range. Energy driven thrombin induced strand displacement and non-enzyme catalyst recycling DNA machine were used to amplify the signal. With the aid of dual-signaling amplification method and the simple signal transduction process, the proposed biosensor exhibited remarkable advantages including perfect analytical capability, ease of fabrication and straightforward operation. This designed aptasensor displayed an extremely low LOD, a wide dynamic range, good selectivity, acceptable stability and can be used for the detection of thrombin in complex samples. Herein, the proposed aptasensor will not only expand the application of isothermal amplification of nucleic acid, but also provide an attractive way to detect other targets by simply altering the corresponding DNA sequences.

Conflicts of interest

There are no conflicts to declare.

Acknowledgements

This research was supported by the National Natural Science Foundation of China (Grant No. 81802110 and 81902169), the Education Department of Sichuan Province (Grant No. 18ZB0645) and Southwest Medical University (Grant No. 2017102 and 2017103).

References

1 K. A. Tanaka, N. S. Key and J. H. Levy, *Anesth. Analg.*, 2009, **108**, 1433–1446.
2 M. S. Chatterjee, W. S. Denney, H. Jing and S. L. Diamond, *PLoS Comput. Biol.*, 2010, **6**, e1000950.
3 A. D. Kuprash, A. M. Shibeko, R. Vijay, S. C. Nair, A. Srivastava, F. I. Ataullakhanov, M. A. Panteleev and A. N. Balandina, *Biophys. J.*, 2018, **115**, 2461–2473.
4 C. Albayrak, C. A. Jordi, C. Zechner, J. Lin, C. A. Bichsel, M. Khammash and S. Tay, *Mol. Cell*, 2016, **61**, 914–924.
5 B. K. Erickson, C. M. Rose, C. R. Braun, A. R. Erickson, J. Knott, G. C. McAlister, M. Wühr, J. A. Paulo, R. A. Everley and S. P. Gygi, *Mol. Cell*, 2017, **65**, 361–370.
6 Y. Liu, D. Jiang, X. Lu, W. Wang, Y. Xu and Q. He, *J. Agric. Food Chem.*, 2016, **64**, 7882–7889.
7 I. Hmila, M. Wongphatcharachai, N. Laamiri, R. Aouini, B. Marnissi, M. Arbi, S. Sreevatsan and A. Ghram, *J. Virol. Methods*, 2017, **243**, 83–91.
8 H. Deng and Z. Gao, *Anal. Chim. Acta*, 2015, **853**, 30–45.
9 S. Wang, X. Li, B. Jiang, R. Yuan and Y. Xiang, *Sens. Actuators, B*, 2019, **298**, 126929.
10 F. Wu, W. Liu, S. Yang, Q. Yao, Y. Chen, X. Weng and X. Zhou, *J. Photochem. Photobiol., A*, 2018, **355**, 114–119.

11 B. Li, L. Qin, J. Zhou, X. Cai, G. Lai and A. Yu, *Analyst*, 2019, **144**, 5003–5009.
12 W. Yun, N. Li, R. Wang, L. Yang, L. Chen and Y. Tang, *Anal. Chim. Acta*, 2019, **1064**, 104–111.
13 I. Ramsay, R. L. Gorton, M. Patel, S. Workman, A. Symes, T. Haque, D. Irish, S. L. Seneviratne, S. O. Burns and E. Wey, *Clin. Infect. Dis.*, 2016, **63**, 57–63.
14 Z. Liu, W. Qi and G. Xu, *Chem. Soc. Rev.*, 2015, **44**, 3117–3142.
15 A. Hagan and T. Zuchner, *Anal. Bioanal. Chem.*, 2011, **400**, 2847–2864.
16 Y. Wang, F. Wang, Z. Han, K. Huang, X. Wang, Z. Liu, S. Wang and Y. Lu, *Sens. Actuators, B*, 2020, **304**, 127418.
17 Y. Qi, Y. Chen, F.-R. Xiu and J. Hou, *Sens. Actuators, B*, 2020, **304**, 127359.
18 H.-M. Meng, H. Liu, H. Kuai, R. Peng, L. Mo and X.-B. Zhang, *Chem. Soc. Rev.*, 2016, **45**, 2583–2602.
19 C. Yin, D. Jiang, D. Xiao and C. Zhou, *Analyst*, 2020, **6**(145), 2219.
20 G. Maduraiveeran, M. Sasidharan and V. Ganesan, *Biosens. Bioelectron.*, 2018, **103**, 113–129.
21 L. Farzin, M. Shamsipur, L. Samandari and S. Sheibani, *Microchim. Acta*, 2018, **185**, 276.
22 O. Gusev, Y. Hayashizaki and K. Usui, in *Clinical Relevance of Genetic Factors in Pulmonary Diseases*, Springer, 2018, pp. 333–344.
23 X. Ye, Y. Li, L. Wang, X. Fang and J. Kong, *Chem. Commun.*, 2018, **54**, 10562–10565.
24 A. Gahlaut, V. Hooda, V. Dhull and V. Hooda, *Artif. Cells, Nanomed., Biotechnol.*, 2018, **46**, 472–481.
25 B.-Z. Chi, R.-P. Liang, Y.-H. Yuan, L. Zhang, Z.-M. Li and J.-D. Qiu, *Microchim. Acta*, 2018, **185**, 280.
26 Y. Dai, A. Furst and C. C. Liu, *Trends Biotechnol.*, 2019, **37**, 1367.
27 F. C. Simmel, B. Yurke and H. R. Singh, *Chem. Rev.*, 2019, **119**, 6326–6369.
28 W. Zhao, H. Li, Y. Tang, M. Liu, S. Wang and R. Yu, *Microchim. Acta*, 2019, **186**, 517.
29 Z. Zhang, J. Li, J. Yao, T. Wang, D. Yin, Z. Chen and G. Xie, *Biosens. Bioelectron.*, 2016, **79**, 488–494.
30 B. Yurke, A. J. Turberfield, A. P. Mills Jr., F. C. Simmel and J. L. Neumann, *Nature*, 2000, **406**, 605.
31 P. Yin, H. M. Choi, C. R. Calvert and N. A. Pierce, *Nature*, 2008, **451**, 318.
32 B. Li, A. D. Ellington and X. Chen, *Nucleic Acids Res.*, 2011, **39**, e110.
33 J. Yao, Z. Zhang, Z. Deng, Y. Wang and Y. Guo, *Analyst*, 2017, **142**, 4116–4123.
34 N. R. Markham and M. Zuker, in *Bioinformatics*, Springer, 2008, pp. 3–31.
35 D. Y. Zhang, S. X. Chen and P. Yin, *Nat. Chem.*, 2012, **4**, 208.